

TAILORING OF THE RF-PROPERTIES OF A MULTICHANNEL ACCELERATOR FOR MeV-ENERGIES

R.G.C. Wojke, R.J.J.M. Steenvoorden, W.H. Urbanus and J.G. Bannenberg, Association EURATOM-FOM, FOM-Institute for Atomic and Molecular Physics, Kruislaan 407, 1098 SJ Amsterdam, The Netherlands,

H. Klein, A. Schempp, R.W. Thomae and T. Weis, Institute for Applied Physics, University Frankfurt, Robert-Mayer-Straße 2-4, 6000 Frankfurt/Main, Federal Republic of Germany,

P.W. van Amersfoort, Association EURATOM-FOM, FOM-Institute for Plasma Physics, Edisonbaan 14, 3439 NM Nieuwegein, The Netherlands.

**Abstract:** Measurements on the rf properties of a modified Interdigital-H-resonator equipped with a multichannel, low- $\beta$  acceleration structure (MEQALAC) are compared with model calculations. The standard description of such a capacitively loaded resonator by a lumped-circuit model is improved by a more extended model. In this model the resonator is treated as a series of inductively coupled circuits containing the components of the separate resonator cells. This way, the local properties of the resonator are taken into account, so that the functional dependence of the voltage distribution over the rf gaps on the resonator geometry can be found. The results are reasonably consistent with measurements.

**Introduction**

An approach to the production of intense ion beams in the sub-Ampere current range is the Multiple Electrostatic Quadrupole Array Linear Accelerator, MEQALAC, which was proposed by Maschke.<sup>1</sup> In this device the ions are accelerated in a sequence of rf gaps and radially focused by electrostatic quadrupoles. Thus, the rf power coupled into the resonator is completely used for acceleration, giving the MEQALAC an intrinsically high acceleration efficiency. An additional advantage is that the longitudinal and the transverse field can be independently optimized. Via the special arrangement of the quadrupole elements it is possible to stack many beams within a small area. This way, the total accelerated current can be increased via an increase of the number of beams.

The MEQALAC project at the FOM-Institute in Amsterdam consist of two stages. In our proof-of-principle experiment, called 'Stage I', a maximum He<sup>+</sup>-ion current of 2.2 mA per channel was accelerated from 40 keV to 116 keV through four parallel channels in a cylindrical resonator cavity.<sup>2</sup> A follow-up experiment, called 'Stage II', is presently under construction. We will accelerate four N<sup>+</sup>-ion beams to 1 MeV in a new cavity with rectangular cross section and exchangeable side plates, which enables to vary the resonator inductance, and thus the resonance frequency. This opens the possibility to vary the exit energy.<sup>3</sup>

The set-up consists of a bucket-type ion source at 40 kV, a four-grid extraction system, a radial matching section, a Low Energy Beam Transport (LEBT) section including a buncher, and an accelerating section. The latter utilizes a modified Interdigital-H-resonator which is excited in the TE<sub>111</sub> mode. When this ground mode is excited, the rf current flows over the support boxes and the circumference of the cavity as indicated in fig. 1. The rf magnetic field flows around the support boxes. These boxes face each other in the form of two 'meander'-like structures, forming the accelerating gaps. Because the magnetic field must have space to turn around, the end plates closing the resonator are located at some distance from the support boxes.

**The circuit model**

An elementary model is discussed in detail by Thomae et al.<sup>4</sup> We present a more detailed model in which the resonator is treated as a series of N cells with label n, see fig. 2. Each cell contains one rf gap. In terms of circuit elements it consists of a single capacitance C<sub>n</sub>, two inductances L<sub>n</sub> and two resistances R<sub>n</sub>. The cells representing the first (n=1) and the last (n=N) cell in the accelerating structure contain only a single inductance and a single resistance.

The procedure for the determination of the rf properties can be out-

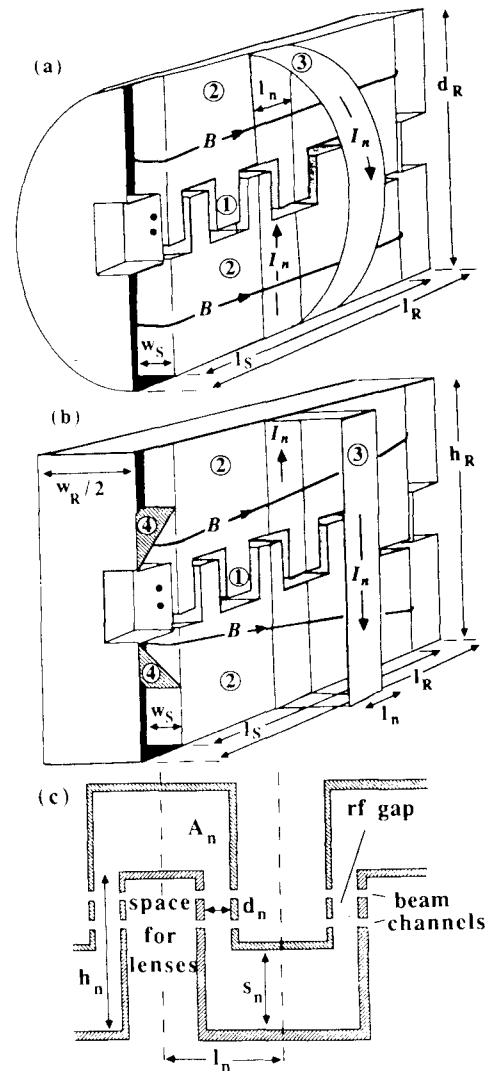


Fig. 1. Cross-sectional view of the MEQALAC resonator: (a) - cylindrical Stage-I resonator, (b) - rectangular Stage-II resonator including shorting plates (4), (c) - details of the meander structure. The ions are accelerated in a meander-like gap structure (1). The rf magnetic field, B, flows around the support boxes (2) onto which the meanders are mounted. The path of the corresponding radial current through cell n, I<sub>n</sub>, is indicated (3). Electrostatic quadrupole lenses are mounted inside the hollow 'fingers' of the meander structure.

lined as follows. First, C<sub>n</sub>, L<sub>n</sub> and R<sub>n</sub> are straightforwardly calculated, and the mutual inductances are estimated from the resonator geometry. These values are inserted into the Kirchhoff equations. Assuming harmonic oscillation we end up with 2N linear equations, where the 2N coefficients determine the amplitude and phase of the rf current and voltage in each cell. The equations are solved for a guess value of the resonance frequency, after which the total rf voltage (i.e. the sum of the individual gap voltages) can be computed. This procedure is repeated for varying frequency until the total rf voltage has its maximum value; resonance is then, by definition, attained.

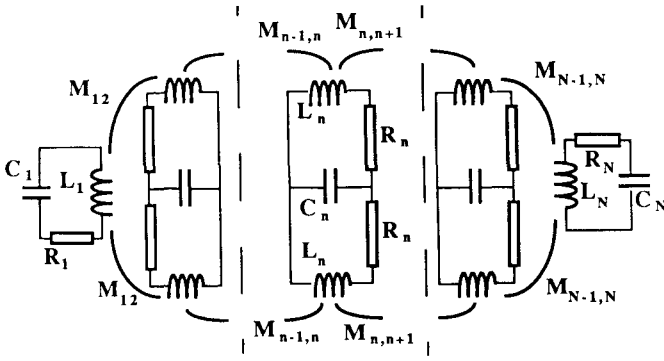


Fig. 2. The circuit model representing the MEQALAC resonator.

The cell capacitance,  $C_n$ , is given by

$$C_n = \epsilon_0 \left( \frac{A_{gn}}{d_n} + \frac{A_{hn}}{s_n} \right), \quad (1)$$

$A_{gn}$  and  $A_{hn}$  are the vertical and horizontal surfaces in the meander structure, respectively, forming the capacitances;  $d_n$  and  $s_n$  are the distances in between, see fig. 1. The cell resistance is given by

$$R_n = \sqrt{\frac{\rho \omega \mu_0}{2}} r \frac{S_n}{l_n}, \quad (2)$$

with  $\rho$  denoting the specific resistance,  $\omega$  the angular frequency,  $\mu_0$  the permeability of vacuum,  $S_n$  the length of the radial current path, and  $l_n$  its width, see fig. 1. The resistance enhancement factor, due to the surface roughness for machined surfaces, has the value  $r=2.4$

The existing formulas of the cell inductances are only rough approximations and their regime of validity is limited.<sup>5</sup> Therefore we use the expression

$$L_n = \left\{ \mu_0 \frac{A}{\langle l_n \rangle} \right\} c_1 \left\{ \frac{\langle l_n \rangle}{l_n} \right\}^\epsilon, \quad (3)$$

in which  $A$  is the cross section and  $l_n$  the length,  $c_1$  is a fit parameter,  $\langle l_n \rangle$  is the average cell length, and  $\epsilon$  is a constant. The first term between brackets gives the inductance of a long solenoid, the second term introduces the dependence of the length. For  $c_1=1$  and  $\epsilon=0.25$  we obtain good agreement with the  $l_n$ -dependence observed in inductance measurements on two 'free standing' current loops with  $l=1.7$  cm and  $l=7.1$  cm, respectively, and  $A=0.2$  m<sup>2</sup> (which corresponds to the second and last but one cell of Stage II). Eq. (3) was checked for 'free standing' current loops, i.e., for loops far away from any metallic environment. However, the current loops in our model are part of a metallic resonator, which leads to the much more homogeneous magnetic field which has been measured for Stage I and Stage II. This is expected to cause a strong decrease of the inductance. Consequently,  $c_1$  is expected to have a value much smaller than one. Indeed, in adjusting  $c_1$  such that the measured resonance frequency coincides with the experimental value, we find that  $c_1=0.061$  for Stage I and 0.052 for Stage II, assuming  $\epsilon=0.25$ . The small difference between these values is due to the different geometry.

The cells are coupled via the mutual inductances  $M_{nm}$

$$M_{nm} = k_{nm} \sqrt{L_n L_m}, \quad (4)$$

where the coupling factor between cell  $n$  and cell  $m$  is defined as  $k_{nm} = \phi_n / \phi_m$ , with the magnetic flux through the cell in question denoted as  $\phi$ . The coupling factor must obey the dependences  $k_{nm}=1$  for  $n=m$ ,  $k_{nm}<1$  for  $n \neq m$ . Further,  $k_{nm}$  should decrease with increasing free area  $\Sigma A_n$  between the cells in question, thus

$$k_{nm} = \left\{ \sum_1^N A_n - \sum_n^m A_n \right\} / \sum_1^N A_n \quad (5)$$

where the last sum is the total free area in the accelerating structure.

The voltages  $U_C$ ,  $U_L$  and  $U_R$  over the corresponding circuit elements  $C_n$ ,  $L_n$  and  $R_n$  in cell  $n$  are governed by the equations

$$C_n \frac{dU_C}{dt} = \alpha I_n \quad (6)$$

$$U_L = \sum_{m=1}^N M_{nm} \frac{dI_m}{dt} \quad (7)$$

$$U_R = R_n I_n \quad (8)$$

with  $\alpha=1$  for  $n=1$  and  $n=N$ , and  $\alpha=2$  for  $1 < n < N$ . The voltages are coupled via the Kirchhoff equation

$$U_C + U_L + U_R = U_0 \cos \omega t, \quad (9)$$

where  $U_0 \cos \omega t$  is the externally induced voltage in cell  $n$ . If we try the general solution

$$I_n = p_n \cos \omega t + q_n \sin \omega t \quad (10)$$

for the current in eqs. (6)-(8), and select the coefficients of the terms containing a sine and a cosine, respectively, we end up with the equations

$$\sum_{m=1}^N [(M_{nm} \omega^2 C_n - \alpha \delta_{mn}) p_m] - \omega R_n C_n q_n = 0, \quad (11.a)$$

$$\sum_{m=1}^N [(M_{nm} \omega^2 C_n - \alpha \delta_{mn}) q_m] - \omega R_n C_n p_n = \omega C_n U_0 \quad (11.b)$$

$\delta_{mn}$  denotes the delta function ( $\delta_{mn}=0$  for  $n \neq m$  and  $\delta_{mn}=1$  for  $n=m$ ). For a network of  $N$  cells,  $2N$  linear equations similar to eqs. (11) are obtained. They contain  $2N$  unknown variables, namely all  $p_n$  and  $q_n$ .

The voltage  $U_C$  in gap  $n$  is obtained by substituting eq. (10) into eq. (6) and integrating over time,

$$U_C = U_n \sin(\omega t + \psi_n), \quad (12)$$

$$U_n = \alpha \frac{\sqrt{p_n^2 + q_n^2}}{\omega C_n} \quad (12.a)$$

$$\psi_n = -\frac{p_n}{q_n} \quad (12.b)$$

denoting the maximum gap voltage and the phase, respectively. The total voltage in the resonator is the sum over all gap voltages and has its maximum value at resonance, where  $\omega = \omega_0$ . If  $\psi_n$  has the same value in each cell, the maximum voltage in all rf gaps is reached at the same time, namely when  $\omega t + \psi_n = \pi/2$ . Then the stored energy in the resonator is given by

$$E = \sum_{n=1}^N \left\langle \frac{C_n U_n^2}{2} \right\rangle = \sum_{n=1}^N \frac{\alpha^2 (p_n^2 + q_n^2)}{2 \omega^2 C_n} \quad (13)$$

and the total loss power in the resonator is given by

$$P = \sum_{n=1}^N \left\langle \alpha R_n I_n^2 \right\rangle = \sum_{n=1}^N \alpha R_n \frac{p_n^2 + q_n^2}{2}. \quad (14)$$

Now the parallel resonator resistance  $R_p$  and the quality factor  $Q$  can be easily calculated. The first is related to the efficiency with which the rf power coupled into the resonator is converted into accelerating voltage. It is defined as

$$R_p = \left( \sum_{n=1}^N U_n \right)^2 / P \quad (15)$$

The quality factor  $Q$  is a measure for the voltage elevation at resonance and defined as

$$Q = \frac{\omega_0 E}{P}. \quad (16)$$

### Comparison with measurements

The dimensions of the cylindrical Stage-I and the rectangular Stage-II resonator are summarized in table 1. The smaller resonance frequency of the latter as compared to Stage I leads to its increased dimensions.

Taking the fit parameter  $c_1$  in eq. (3) equal to 0.061 and 0.052 for Stage I and Stage II, respectively, we find values for  $R_p$  and  $Q$  which are roughly a factor of two too large, whereas the calculated value for  $R_p/Q$  is quite close to the experimental value: 9.9 k $\Omega$  instead of 9.2 k $\Omega$  for Stage I, and 15.7 k $\Omega$  instead of 15.8 k $\Omega$  for Stage II, respectively, see table 2.

The voltage distribution across the rf gaps, as obtained by perturbation measurements, is shown in fig. 3, together with the calculated distribution. Agreement between measurements and calculations is reasonable.

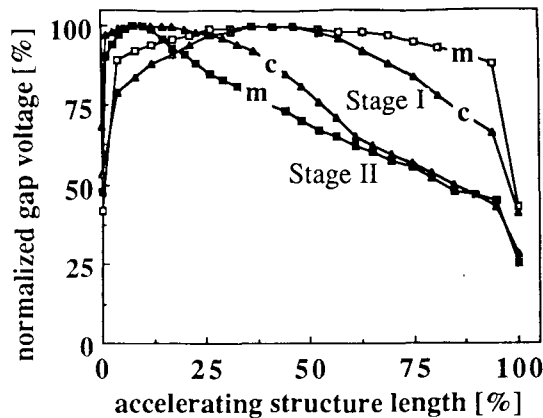


Fig. 3. Measured (m) and calculated (c) voltage distribution across the rf gaps for both the Stage-I resonator and the Stage-II resonator, normalized to their maximum value.

Table 1. Dimensions of the Stage-I and the Stage-II resonator.

		Stage I		Stage II	
Resonance frequency	$\omega_0/2\pi$	40	25		MHz
Resonator diameter	$d_R$	40	-		cm
Resonator height	$h_R$	-	100		cm
Resonator width	$w_R$	-	50		cm
Resonator length	$l_R$	70	170		cm
Accelerating structure length	$l_S$	45	140		cm
Accelerating structure width	$w_S$	7	9		cm
Number of rf gaps	N	20	30		-

Table 2. Rf properties of both the Stage-I resonator, as measured (a) and calculated (b), and the Stage-II resonator, as measured (c) and calculated with the model (d).

	a	b	c	d	
$\omega_0/2\pi$	40.0	40.0	18.2	18.2	MHz
$R_p$	16.5	37.9	25.0	41.8	M $\Omega$
Q	1800	3820	1580	2670	-
$R_p/Q$	9.2	9.9	15.8	15.7	k $\Omega$

For Stage II we remark that the measured resonance frequency is 18.2 MHz rather than the planned 25 MHz; adjustment to the latter value is achieved with shorting plates, which also decrease the gap voltage at the resonator entrance due to a higher transmission. Model calculations with this voltage ramp are presently carried out.

#### Discussions and conclusions

The model yields values for  $R_p$  and Q, which are roughly a factor of two too large, whereas the ratio  $R_p/Q$  is predicted reasonably well. In a somewhat heuristic approximation, Thomae et al.<sup>4</sup> propose to account for this effect by the local inhomogeneity of the magnetic field at the accelerating structure ends and corresponding power losses there. In view of the fact that  $R_p$  and Q are strongly depressed by power losses due to locally increased current densities, whereas  $R_p/Q$  only depends on the resonator geometry, we conclude from this that there are no intrinsically wrong assumptions in the models.

The main advantage of the extended model is that it allows to predict, besides the overall resonator properties, also the voltage and phase distribution over the rf gaps. The calculated voltage distribution is reasonably consistent with measurements. The phase distribution (which cannot be obtained by means of perturbation measurements) is flat within 1 % for both resonators.

Concerning the actual voltage distributions, we note that there is a striking difference between Stage I and Stage II: in Stage I the distribution is nearly flat (apart from the first and the last cell of the structure, which are connected to the 'grounded' resonator body), whereas in Stage II there is a pronounced decrease of the gap voltage at the exit part of the structure, cf. fig. 3. We attribute this observation to the much more homogeneous distribution of gap capacitances in Stage I, which is shown in fig. 4 together with the distribution for Stage II. The latter falls off sharply with increasing rf gap width  $d_n$  in the first part of the accelerator, the increasing cell length  $\beta_n \lambda/2$  causes the increase of the cell capacitance in the second part; note that the increase of  $\beta_n \lambda/2$  is much more pronounced than in Stage I due to the higher exit energy (1 MeV rather than 120 keV). The last rf gap has a higher capacitance because of its reduction of the gap width  $d_n$ .

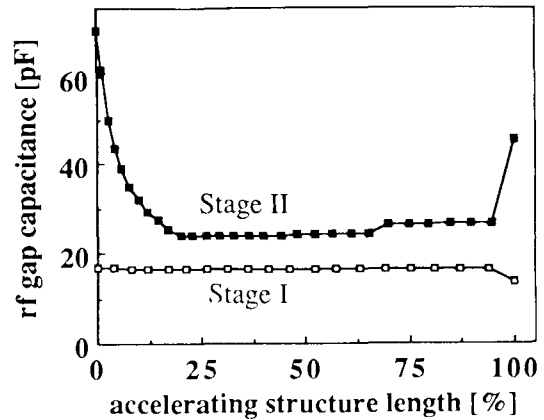


Fig. 4. Distribution of the gap capacitances along the Stage-I and the Stage-II structure.

Returning to our model calculations, we conclude that they provide a reasonably powerful tool to predict the resonator properties. However, the model requires knowledge of the resonance frequency in order to adjust  $c_1$  in eq. (3). These parameters must be obtained from rf measurements (e. g. on a scale model).

#### Acknowledgements

This work was performed as part of the association agreement between the Stichting voor Fundamenteel Onderzoek der Materie (FOM) and EURATOM, with financial support from the Nederlandse Organisatie voor Wetenschappelijk Onderzoek (NWO), the Nederlandse Ministerie van Onderwijs en Wetenschappen, and EURATOM.

#### References

- 1 A.W. Maschke, Brookhaven Nat. Lab. Rep. BNL-51209 (1979).
- 2 R.W. Thomae, F. Siebenlist, P.W. van Amersfoort, E.H.A. Granneman, H. Klein, A. Schempp and T. Weis, J. Appl. Phys. 62(1987) 4335.
- 3 P.W. van Amersfoort, R.G.C. Wojke, W.H. Urbanus, A.E. van Putten, R.J.J.M. Steenvoorden, H. Klein, A. Schempp and T. Weis, Proc. of 1987 IEEE Part. Acc. Conf., E.R. Lindstrom, L.S. Taylor, IEEE, New York (1987) 340.
- 4 R.W. Thomae, F. Siebenlist, P.W. van Amersfoort, E.H.A. Granneman, H. Klein, A. Schempp and T. Weis, Nucl. Instr. and Meth. in Phys. Res., A251 (1986) 211.
- 5 H. Meinke, F.W. Gundlach, Taschenbuch der Hochfrequenztechnik, Springer Verlag, Berlin, Göttingen, Heidelberg, (1962) 15.